Mechanical Zonation of Rock Properties and the Development of Hydrothermal Fluid Circulation Pathways: Implications for Enhanced Geothermal Systems

Oladoyin Kolawole (doyin.kolawole@ttu.edu)
Bob L. Herd Department of Petroleum Engineering, Texas Tech University https://orcid.org/0000-0001-9202-172X

Ion Ispas
Texas Tech University

Folarin Kolawole
School of Geosciences, University of Oklahoma

Christophe Germay
EPSLOG S.A

John D McLennan
Department of Chemical Engineering, University of Utah

Research

Keywords: Enhanced geothermal system, Geomechanics, Hydrothermal alteration, Mechanical stratigraphy, Fracture mechanics

Posted Date: December 10th, 2020

DOI: https://doi.org/10.21203/rs.3.rs-122204/v1

Mechanical Zonation of Rock Properties and the Development of Hydrothermal Fluid Circulation Pathways: Implications for Enhanced Geothermal Systems

Oladoyin Kolawole[1,2]*, Ion Ispas[1,2], Folarin Kolawole[3,4], Christophe Germay[5], John D. McLennan[6]

[1]*Rock Mechanics Laboratory, 101 Terry Fuller Petroleum Engineering Research Building, Texas Tech University, Lubbock, TX, USA*

[2]*Bob L. Herd Department of Petroleum Engineering, Texas Tech University, Lubbock, TX, USA*

[3]*School of Geosciences, University of Oklahoma, Norman, OK, USA*

[4]*Now at BP America Inc., Houston, TX, USA*

[5]*EPSLOG S.A., Liege, Belgium*

[6]*Department of Chemical Engineering, University of Utah, Salt Lake City, UT, USA*

*Corresponding author: doyin.kolawole@ttu.edu (Oladoyin Kolawole)

ORCID: O.K - 0000-0001-9202-172X; I.I - 0000-0003-3426-4031; F.K - 0000-0002-5695-2778; JD.M - 0000-0002-6663-5063

ABSTRACT

Oil and gas operations in sedimentary basins have revealed significant temperatures at depth, raising the possibility of major geothermal resource potential in the sedimentary sequences. The efficient development of such a resource may require enhancement by hydraulic stimulation. However, effective stimulation relies on an initial assessment of in-situ mechanical properties and a Discrete Fracture Network (DFN) model of the rock response. Here, we examine the distribution of mechanical properties (unconfined compressive strength, *UCS*; ultrasonic velocity-derived Poisson ratio, ν; and, scratch-derived fracture toughness, K_s) along the cored interval of a sedimentary formation with a known geothermal anomaly in the Permian Basin, U.S. Our results reveal the mechanical heterogeneity of the rock, demonstrated by four distinct alternating mechanical zones, which include: (1.) mechanically weaker 0.17 m-thick Zone-A and 0.18 m-thick Zone-C with mean

UCS = 110 MPa, ν = 0.25, K_s = 1.89 MPa·√m; and (2.) mechanically stronger 0.41 m-thick Zone-B and 0.15 m-thick Zone-D which show mean *UCS* = 166 MPa, ν = 0.22, and K_s = 2.87 MPa·√m. Although X-ray Diffraction analyses of the samples suggest that the entire rock matrix is dominated by dolomite, the stronger zones show a higher abundance of quartz (>30%) and relatively lower phyllosilicate mineral content (<2%) than the weaker zones. Further, we observe that the mechanically stronger zones have the greatest occurrences of hydrothermal alterations (anhydrite veins and nodules), indicating that the cored interval had experienced hydrothermal fluid circulation in the past. We infer that the denser clustering of fractures in the stronger zones which facilitated the hydrothermal vein development was due to the influence of mechanical stratigraphy on the brittle deformation and alteration of the sedimentary-hosted hydrothermal reservoir. Thus, we suggest that the stronger zones represent viable targets for hydraulic stimulation of a geothermal reservoir, both for the emplacement of new fractures and the linkage of pre-existing fractures. Our findings in this study provide an analog for hydraulic stimulation of viable geothermal reservoir targets at higher in-situ temperatures and higher geothermal gradients.

Keywords: Enhanced geothermal system; Geomechanics; Hydrothermal alteration; Mechanical stratigraphy; Fracture mechanics

1. Introduction

Enhanced geothermal systems (EGS) are reservoirs that have been stimulated to efficiently extract heat from low permeability high-temperature rocks (Nadimi et al. 2020). Hydraulic fracturing is one of the most efficient stimulation techniques currently considered for heat extraction from an EGS, through the injection of highly pressurized fluid into the formation to initiate and propagate or reactivate natural fractures. Hydraulic fractures (HF) play an important role in improving the heat extraction performance of an EGS (Murphy et al. 1977; Campbell et al. 1981; Zhou et al. 2018; Zhang et al. 2020). In assessing a viable geothermal reservoir, three important components are required for consideration, and they are heat, mobile fluid, and permeability (Nadimi et al. 2020). Reactivation of pre-existing natural

fractures (NF) induced by injection fluid has become widely accepted as an important mechanism for fracture network connectivity and permeability enhancement in EGS reservoirs (Pine and Batchelor 1984; McClure and Horne 2013; Finnila et al. 2015; Sheng et al. 2018). Various EGS stimulation mechanisms have been proposed, based on field observation and laboratory programs. Specific mechanisms depend on the geology, in-situ stress, fault structures, and pre-existing natural fractures (McClure and Horne 2014; Nadimi et al. 2020).

Studies have shown that EGS is characterized by heterogeneous geology, which includes pre-existing fracture networks that are mineralized (Callahan et al. 2019a, 2019b, 2020). It is also known that during hydraulic fracturing stimulation, propagating hydraulic fractures are known to link and connect pre-existing natural fractures (NF) (Kolawole and Ispas 2020a). During a hydraulic fracturing treatment, complex fracture networks are often generated, and the HF-NF interaction significantly influences the complexity of the networks created. Some of these pre-existing natural fractures include veins, and their reactivation can result in induced seismicity (Kolawole et al. 2019). Veins are open fractures that are occluded minerals.

Drilling, completion, injection, and production from very deep, High-Temperature High-Pressure (HPHT) reservoirs is an expensive operation, and its success demands an understanding of the in-situ rock mechanical properties. These rock mechanical properties have implications for subsurface energy (oil and gas) exploration, recovery of high-temperature fluids from geothermal reservoirs (Toth 2020), and geological CO_2 storage (GCS). The behavior of fractured, low-permeability reservoirs, as in an EGS setting, is a critical consideration in achieving the successful extraction of resources from such reservoirs (Crandall et al. 2019).

Modeling and prediction of in-situ rock failure behavior as a function of rock type, pore pressure, spatio-temporal stresses, and fault-reactivation potential provide critical information for proactive decision-making to achieve successful energy production and heat extraction operations (Dotsey and Deighton 2012; Wang and Ghassemi 2012; Stober and Bucher 2013; Shao et al. 2016; Nadimi et al. 2020; Zhang et al. 2020; Ziegler and Heidbach

2020). In addition, the post-primary mineral precipitation during hydrothermal alterations has a significant impact on the mechanical properties of a geothermal reservoir (Meller and Kohl 2014). However, the rock mechanical properties of EGS reservoirs adopted in numerical models are often overestimated since the effects of pre-existing NF and geological heterogeneity are often not fully accounted for (Frash et al. 2013; Gholizadeh Doonechaly et al. 2013; Riahi et al. 2015; Han et al. 2019; Ishibashi et al. 2019). Therefore, there is a need to better constrain the modeling of the rock mechanical response due to the pre-existing geological heterogeneity of target geothermal reservoirs, by considering its geomechanical and mineralogical properties, in addition to its fractomechanical behavior.

Here, we examine the distribution of mechanical properties along the cored interval of a high-temperature sedimentary formation, and the implications for the extraction of heat from a target EGS reservoir. We utilize the Scratch Test method to characterize the mechanical properties of a core from a potential geothermal area in the Central Basin Platform of the Permian Basin, United States. Our results show heterogeneous mineralogy and rock strength distributions over the core length, with alternating mechanically weak and strong intervals. Further, we find denser clustering of fractures in the stronger zones the cored intervals (1705.12 – 1705.53 m and 1705.71 – 1705.86 m) which facilitated the hydrothermal vein development, was due to the influence of mechanical stratigraphy on the brittle deformation and alteration of the sedimentary-hosted hydrothermal reservoir. Our findings in this study provide an analog for hydraulic stimulation of viable geothermal reservoir targets at higher in-situ temperatures and higher geothermal gradients.

2. Permian Basin Geothermal Areas

The Permian Basin is a large (220,000 km^2) Late Paleozoic sedimentary basin, spanning parts of West Texas and Southeastern New Mexico, United States. The Permian Basin is composed of three smaller components known as the Delaware Basin, the Central Basin Platform, and the Midland Basin (Tang 2015). The Central Basin Platform, which lies between the Midland and Delaware Basins, is a zone of Permian tectonic uplift and hosts a significant sequence of carbonate reservoir units, and has a geothermal gradient in the range

of 23.04 – 28.51 °C/km (Erdlac Jr and Swift 2004; Ruppel et al. 2005). Among these is the prominent San Andres Formation which is known to have an average porosity of ~7% and permeability in the range of 1-100 mD (Saller et al. 2012). Nodular anhydrites are pervasive in the Permian Basin sedimentary sequences and occur in varying degrees of clustering within the stratigraphy (Kerr Jr and Thomson 1963). Post-deposition of the carbonate sequences, the anhydrite nodules were precipitated by the thermally-driven circulation of highly-charged groundwater within the basin (Kerr Jr and Thomson 1963).

Geothermal areas (G.A.) have been identified in the Permian Basin (Erdlac Jr and Swift 2004; Erdlac Jr 2006) among which three are most prominent (Fig. 1a; Erdlac Jr 2006). These fields with known geothermal anomalies are characterized by 32 - 71 °C hydrothermal systems occurring at ~152 – 1,524 m depths within the sedimentary sequences (Erdlac Jr 2006). The hot water from these fields might have value for direct heat or heat pump applications because a minimum of 150 °C is required at reservoir depth for an ORMAT-type Organic Rankine Cycle (ORC) plant (Kaplan 2007; Quoilin et al. 2013). The northernmost of the three herein referred to as the Northern G.A., straddles the northwestern Midland Basin and the northeastern corner of the Central Basin Platform. The other geothermal areas include the "Southern G.A." and "Southwest G.A.", located in the southern Central Basin Platform and SW Delaware Basin, respectively.

3. Data & Methodology

3.1 Core Data

The core sample analyzed in this study is 0.91 m-long, obtained from a deep carbonate interval in the southern portion of the Northwestern Shelf and near the northernmost part of the Central Basin Platform; a location which corresponds to the SW tip of the Northern G.A. Although these potential geothermal reservoirs are estimated to occur at ~152 – 1,524 m depths (Erdlac Jr 2006), we note that our core sample extends over to a slightly deeper interval of 1705.0 – 1705.9 m, and we believe it is representative because it provides a higher geothermal gradient than in previously reported studies.

We conducted X-ray diffraction (XRD) analyses for different portions of the sample to evaluate the mineralogical characteristics of the core. More specifically, we analyzed portions of the rock matrix in the shallowest (1705.0 m) and deepest (1705.9 m) sections of the core. Along the entire core, we observe the presence of nodules and veins of varying sizes/thicknesses, characterized by light-colored mineralization. We obtained a sample from the most prominent one of these nodules (0.02 m-thick) (Fig. 2; SF. 1, Supplementary Information) and performed an XRD analysis in order to determine its composition. All the samples were measured in whole-rock condition from 3.5 to 70° 2Θ at 40 V/40 A, 1.5 sec per step with a 1mm divergent slit. In addition, we performed a core-scale characterization of the post-diagenetic alterations in the rock, which included the distribution of open-fractures, mineralized veins, and nodules. Post-diagenetic alterations refer to changes in the rock after lithification (a process where sediments are compacted and cemented to form rock). Therefore, in this study, we refer to post-diagenetic alteration as secondary alterations in the rock.

3.2 Estimation of Rock Strength using the Scratch Test

The scratch test is a quasi-non-destructive method based on pushing a tool (cutter) across the surface of a rock at a given penetration depth (Kolawole and Ispas 2020b). The scratch test method is useful in estimating reservoir geomechanical and petrophysical properties (Detournay and Defourny 1992; Schei et al. 2000; Mitaim et al. 2004; Coudyzer et al. 2005; Dagrain and Germay 2006; Dagrain et al. 2006; Richard et al. 2012; Germay et al. 2015, 2018). The scratch test method (Fig. 3a) measures horizontal (F_T) and vertical (F_V) forces exerted during the so-called scratching and infers the unconfined compressive strength (*UCS*). Ultrasonic compressional and shear velocities (V_p and V_S) are used to calculate a dynamic Poisson's ratio (ν). The horizontal scratch force (F_T) is used to calculate the scratch-derived fracture toughness (K_s). The dynamic Poisson's ratio and the *UCS* were independently measured on plugs taken from the same core.

In the scratch tests, a continuous groove in the rock surface is created with a cutting tool. The cutter penetration depth (d) and the cutter velocity (v) relative to the rock are held constant. The horizontal force (F_T) is parallel to the cutter velocity, and the vertical force

(F_V) is perpendicular to the cutter velocity. The intrinsic specific energy (ε) is the energy required to scratch a unit volume of rock (Detournay and Defourny 1992; Suarez-Rivera et al. 2002). ε is presumed to be a rock property characteristic that directly correlates to the rock's unconfined compressive strength (*UCS*). The scratch cutter-rock interaction model (Detournay and Defourny 1992) and its application to estimate rock strength, combining pure cutting and frictional contact processes are presented in Eq. 1- 6 (for a rectangular cutter) as:

$$F_T = \varepsilon(1 - \mu\zeta)wd + F_V \quad (1)$$

$$\mu = \tan\phi \quad (2)$$

$$E = E_o + \mu S \quad (3)$$

$$E_o = \varepsilon(1 - \mu\zeta) \quad (4)$$

$$E = \frac{F_T}{wd} \quad (5)$$

$$S = \frac{F_V}{wd} \quad (6)$$

where: w is the width of the cutter; d is the cutter penetration depth; ε is the intrinsic specific energy; ζ is the inclination of the average force acting on the face of the cutter; and μ is the coefficient of friction on the wear flat/rock interface; ϕ is the internal friction angle of the rock; S is the drilling strength of the cutter; and E is the specific energy.

In this study, we used the Wombat scratch machine (Fig. 3b) to scratch our candidate core. The features of the polycrystalline diamond compact (PDC) cutter used for the scratching include a rectangular-shaped, sharp, flat, with a width (w) of 10 mm, and back-rake angle (θ) of 15°. The V_p and V_s were measured perpendicular to the long axis of the core. In addition, the scratch equipment allows us to acquire an ultra-high-definition panoramic photograph of the full scratch length along the core sample. We used a cylindrical core sample 0.914 m long and 0.1 m in diameter, cut nominally perpendicular to the bedding plane. The core sample was obtained from a depth of 1705 m in a well in the northern part of the Central Basin Platform, Permian Basin, U.S. We conducted scratch tests on the core sample at cutter

200 penetration depths (d) of 0.05 mm, 0.08 mm, 0.11 mm, 0.14 mm, 0.17 mm, 0.20 mm, 0.23
201 mm, 0.26 mm, and 0.29 mm.

202 The data obtained from the scratch test allow us to calculate the scratch toughness (K_s) and
203 Poisson's ratio (ν) values along the core. K_s, with units of MPa·√m, is an estimate of the
204 fracture toughness (K_{IC}) of a rock (Akono 2013; Akono and Kabir 2016), given by the
205 following relationships:

206 $$K_s = \frac{F_T}{\sqrt{2pA_c}} \quad \left[MPa\sqrt{m}\right] \tag{7}$$

207 Where: A_c is the contact area due to horizontal force (F_T) in the scratch direction for a
208 rectangular-shaped cutter, and p is the fracture surface perimeter for a cutter width (w) at
209 maximum cutting depth (d). We note that the experiments performed in this study were
210 done at ambient room temperature and unconfined stress conditions.

211

212 **4. Results**

213 *4.1 Core Characterization and XRD Analysis*

214 The XRD analyses of the rock matrix (samples from the shallowest and deepest parts of the
215 core) show that the rock is a dolostone, dominated by dolomite, with varying concentrations
216 of quartz, muscovite, illite, chlorite, and anhydrite (Fig. 4a). However, the analyses also show
217 that the nodule sample is composed of anhydrite with minor quartz and dolomite (Fig. 4a).
218 This suggests that the nodules and veins of light-colored mineralization observed in the core
219 sample (Fig. 4b) are composed of anhydrites. Overall, we find that the greatest clustering of
220 the anhydrite veins and nodules occur within a 0.41 m-thick interval in the central part of
221 the core. However, the open-fractures appear to be evenly distributed along the core length,
222 and since the opened-fractures pre-existed in-situ, we suspect they might be opened due to
223 stress relaxation.

224

225 *4.2 Unconfined Compressive Strength (UCS)*

226 A continuous scratch test *UCS* log profile of the full core sample shows that the highest *UCS*
227 values along the core occur at depth intervals of 1705.12 – 1705.53 m (Zone B) and 1705.71

– 1705.86 m (Zone D), and are separated by intervals of relatively lower *UCS* values at 1704.95 – 1705.12 m (Zone A) and 1705.53 – 1705.71 m (Zone C). The color shades (Fig. 4d) indicate variations from low to high strength along the core. We observe that the dark and light blue shades match with the high peaks on the *UCS* log. Likewise, we observe that the red, orange, yellow, and light green shades match the low troughs on the *UCS* log.

4.3 Ultrasonic Velocities (Vp, Vs) and Poisson's Ratio (ν)

The measured ultrasonic shear (V_s) and compressional (V_p) velocities and the corresponding Poisson's ratio along the core show the distribution of heterogeneous mechanical properties along the core (Fig. 4e). Although the measured velocities show variations along the core, the calculated Poisson's ratio distribution is most salient. In general, similar to the distribution of *UCS*, we observe that the mechanical Zones A and C show relatively higher Poisson's ratios compared to the intervening Zones B and D (Fig. 4e).

4.4 Scratch Toughness (K_S)

We present the estimates of scratch toughness along the core in Fig. 4f. Again, the distribution of the values and the trend of the moving average fitting curve shows there exists a zonation in scratch toughness along the core. Within Zones A and C, K_s shows the least values (as low as 0.46 MPa·√m), whereas, in Zones B and D, the K_S is highest, attaining a maximum of 3.9 MPa·√m. These K_s values are consistent with results in published literature on fracture toughness of a dolomitic rock (Yao et al. 2020) and a carbonate rock (Eddine 2009).

5. Discussion

5.1 Mechanical Zonation within the Analyzed Core Sample

The core characterization (Fig. 4b) correlates with the presence or absence of open-fractures, mineralized veins, and nodules at depths intervals with high and low strengths (Fig. 4d). This suggests an alternation of strong and weak mechanical zones along the core

sample. The extremely-low *UCS* values observed in mechanical Zones A and C are due to the elevated presence of open fractures in these zones. The strongest zones (Zones B and D) in the analyzed core correspond to the highest *UCS*, highest K_s, and lowest Poisson's ratio. These zones B and D are separated by mechanically weaker zones (Zones A and C; Figs. 4d-4f).

Our XRD analyses (Figs. 4a-4b) examined one of the mechanically strong zones (Zone D) and one of the weaker zones (Zone A). The results show that the strong zones are dominated by a mix of dolomite and quartz-rich matrix, whereas the weaker zones are enriched in phyllosilicate minerals (muscovite, chlorite, and illite). Rocks that are rich in phyllosilicate minerals are significantly weaker in comparison to dolomite-rich rocks (Brindley 1981; Tesei et al. 2012). Anhydrite has an estimated *UCS* of 150 MPa, Quartz 200-250 MPa, Dolomite 140 MPa, Muscovite 50-75 MPa, Illite <10 MPa, (Nataraj 1991; Tham et al. 2001; Chen et al. 2004; Dalamarinis et al. 2009; Majdi and Rezaei 2013; Hantler 2015; Wang et al. 2019). Therefore, we suggest that mechanical zonation is controlled by the relative distribution of mineral types along the core. Further, the mechanically stronger zones (0.41 m-thick Zone-B and 0.15 m-thick Zone-D), have a mean *UCS* of 166 MPa, 0.22 ν, and 2.87 MPa·√m K_s, and hydrothermal alterations occur mostly in these zones (Figs. 4a-4d). The mechanically stronger zones contain clusters of anhydrite veins and anhydrite nodules, a lower abundance of phyllosilicate minerals, and minimal presence of open fractures. The mechanically weaker zones (0.17 m-thick Zone-A and 0.18 m-thick Zone-C), have a mean *UCS* of 110 MPa, 0.25 ν, and 1.89 MPa.√m K_s, with the greatest concentration of open fractures in addition to a higher abundance of phyllosilicate minerals present in these zones (Figs. 4a-4d).

5.2 The Implication for the Development of Enhanced Geothermal System (EGS) Reservoir Targets

The mineralogical analyses (Fig. 4a) indicate that this core has been hydrothermally-modified. Previous geologic studies in the Permian Basin have shown that anhydrite nodules and veins had been emplaced during basin-wide circulation of ancient hydro fluids in ancient times (Kerr Jr and Thomson 1963). Anhydrite can occur as a vein-filling mineral in

hydrothermal deposits (Sleep 1991; Teagle et al. 1998). The presence of open and occluded fractures indicate that this formation is a permeable hydrothermal reservoir, at least in the past.

The collocation of anhydrite nodules, open-fractures, and fractures occluded by anhydrite (i.e. veins) indicate that fractures played an important role in the ancient circulation of hydrothermal fluid within the basin. However, our results indicate that the fractures that controlled fluid circulation in the past were preferentially localized in zones B and D of the carbonate formation (Figs. 4c-4e). The pre-alteration pore system controls the heterogeneous properties at depth intervals dominated by nodules and is without veins. The original mechanical property of the reservoir rock controlled the past hydrothermal circulation pathways and will be relevant to the present-day extraction of heat from EGS reservoirs. Although anhydrite is mechanically weaker than the host dolomitic matrix, our result shows that the incorporation of the anhydrite mineralization has not significantly changed the bulk mechanical properties of zones B and D. Locally, the anhydrite nodules may control the mechanical properties, but at bulk-scale, they seem to exert less control. Thus, we envision that the pre-existing bulk zonation of mechanical properties is relevant for the stimulation of EGS target reservoirs, in combination with other relevant completion data.

Rheology of a rock describes the deformation a rock undergoes in response to stress, excluding the fracture (Handin and Carter 1987). The delineation of the strong and weak zones are based on the *UCS* of the rock, which tends to correlate to the stiffness of the mechanical zones (Deere 1968; Palchik 1999, 2011; Yılmaz and Sendır 2002; Al-Shayea 2004; Gokceoglu and Zorlu 2004; Sonmez et al. 2004; Zoback 2010). However, the efficiency of fracture initiation and propagation is dependent on the rheology of the rocks i.e. brittle rocks have a greater efficiency for fracture nucleation and propagation than ductile rocks (Scholz 1968a, 1986b; Yao 2012; Wang 2015, 2016). Also, it has been established that brittle rocks have a lower fracture toughness than ductile rocks (Gunsallus and Kulhawy 1984; Bhagat 1985; Belyadi et al. 2019; Zhang 2019). Fracture toughness is highly dependent on temperature (Al-Shayea 2000; Zhang et al. 2001; Balme 2004; Funatsu 2004; Zhang 2016), implies that fracture toughness data presented in this study (Fig. 4f) may only be

representative of zonation of mechanical properties along the core, and not of the conditions within which the fractures and veins were emplaced.

Therefore, we infer that within the hydrothermal reservoir temperature and pressure conditions at the time of deformation and alteration of the formation being analyzed in this study, the stiffer zones (zones B and D) were more brittle than the less-stiff zones (zones A and C), thus facilitating the preferential localization of greater fracturing in these stiffer zones. Our observations here suggest an influence of mechanical stratigraphy on the brittle deformation and alteration of the sedimentary-hosted hydrothermal reservoir. Additionally, since veins are essentially mineral-filled fractures, the anomalous concentration of veins in zone B indicates a localized clustering of fractures within zone B prior to hydrothermal alteration. Thus, this implies that the mechanical zonation of the rock may likely have influenced the localized development of fracture clusters of zone B.

Furthermore, the exploration of geothermal energy systems has been associated with induced seismicity (Diehl et al. 2017; Wiemer et al. 2017; Cheng and Chen 2018; Zbinden et al. 2020). However, carbonate minerals (calcite and dolomite), are more mechanically susceptible to earthquake nucleation at higher temperatures and pressures such as those relevant for hydrothermal reservoirs (e.g., Carpenter et al. 2014; Kolawole et al. 2019). Therefore, we infer that the dolomite-rich brittle zones (zones B and D) are more susceptible to earthquake generation in the event of anthropogenic stress perturbation.

5.3 Upscaling Core-Scale Observations to Reservoir Scale

Continuous sampling with a Scratch Test machine provides a fine-scale and detailed measurement of mechanical properties along the sample (e.g. data points in Figs. 4d-4f), whereas the larger-scale trends describe the bulk mechanical properties of the rock (e.g., the color contour of *UCS* in Fig. 4d). In this study, we analyzed only 0.91 m-long core within the San Andres reservoir, and we observed this detailed mechanical heterogeneity. Our field of study is not yet proven as a viable EGS field, primarily because a minimum of 150 °C is required at reservoir depth for an ORMAT-type ORC plant. However, there is a need to upscale our results using DFN models, to explicitly model the geomechanical properties and

characterize our observed mechanical heterogeneity at reservoir-scale. In DFN modeling, the mechanical heterogeneity in rock strength, fracture toughness, Poisson's ratio, mineralogy, and pre-existing fractures (open/mineral-devoid, occluded/infilled/veins), should be considered to develop models that accurately predict reservoir-scale and sub-reservoir scale (localized) fractomechanical characteristics. Therefore, our results provide an analog to what would occur in commercial geothermal reservoir settings at higher in-situ temperatures and higher geothermal gradients, in combination with other relevant completion data.

6. Conclusions

In this study, we examine the distribution of mechanical properties (unconfined compressive strength, *UCS*; ultrasonic velocity-derived Poisson ratio, ν; and, scratch-derived fracture toughness, K_s) along the cored interval of a sedimentary formation with a known geothermal anomaly in the Permian Basin, U.S. In addition, we performed a core-scale characterization of the post-diagenetic alterations in the rock, and XRD analyses to further characterize the heterogeneity of the tested core material.

Our findings from this study reveal:

a. The mechanical heterogeneity of the rocks is demonstrated by four distinct alternating mechanical zones, which include: mechanically weaker 0.17 m-thick Zone-A and 0.18 m-thick Zone-C showing mean *UCS* = 110 MPa, ν= 0.25, K_s = 1.89 MPa·√m; and mechanically stronger 0.41 m-thick Zone-B and 0.15 m-thick Zone-D which show mean *UCS* = 166 MPa, ν= 0.22, K_s = 2.87 MPa·√m.
b. A lower abundance of phyllosilicate minerals in mechanically stronger zones, whereas there is a higher abundance of phyllosilicate minerals in mechanically weaker zones.
c. The investigated core experienced hydrothermal alterations facilitated by the localization of permeable fractures within the mechanically stronger zones of the rock.

d. A high degree of formation heterogeneity, characterized by spatial variation of inherited rock mechanical properties and hence the fracture-mechanical behavior, will impact the stimulation and subsequent extraction of heat from Enhanced Geothermal Systems (EGS).
e. There could be a possible mechanical interaction between a propagating hydraulic fracture and the pre-existing open and anhydrite-occluded fractures.
f. The denser clustering of fractures in the stronger zones which facilitated the hydrothermal vein development was due to the influence of mechanical stratigraphy on the brittle deformation and alteration of the sedimentary-hosted hydrothermal reservoir.

In addition, the EGS stimulation models, such as DFN models, should include a heterogeneous rock volume with detailed characteristics of the individual mineralized zones, and mechanical zonation of the rock matrix. Although our study analyzed a 0.91 m-long cored interval, the findings in this study can be upscaled to commercial geothermal reservoir settings at higher in-situ temperatures and higher geothermal gradients, in combination with other relevant completion data.

We suggest that this work provides novel insights into the understanding of how the heterogeneity of mechanical behavior and properties may influence the stimulation and production from EGS reservoirs. Further, the study provides baseline geomechanical properties that can be incorporated into numerical modeling of rock deformations at higher reservoir temperature and pressure conditions.

Availability of data and materials

The datasets generated and/or analyzed during the current study are available in the Mendeley data repository (Kolawole 2020).

Abbreviations

EGS*:* Enhanced Geothermal Systems; G.A.: Geothermal areas; *UCS*: Unconfined compressive strength; ν: ultrasonic velocity-derived Poisson's ratio; K_s: Scratch-derived fracture toughness; DFN: Discrete Fracture Network; GCS: geologic CO_2 storage; V_p: Ultrasonic compressional velocity; V_s: Ultrasonic shear velocity; NF: pre-existing natural fractures; HTHP: High-Temperature High-Pressure; ORC: ORMAT-type Organic Rankine Cycle; XRD: X-ray diffraction.

Acknowledgments

The authors would like to acknowledge Steward Energy II for providing the core used in this study.

Author's contributions

OK and FK conceptualized the project. OK conducted the experimental investigations and processed the data. OK conducted the core-scale characterization with support from FK. OK analyzed and interpreted the data, and wrote the manuscript. FK guided the interpretation of the results, and supported the writing of the manuscript. II, CG, and JDM edited and improved the manuscript. All authors read and approved the final manuscript.

Funding

No external funding was received for this study.

Competing interests

The authors declare that they have no competing interests.

Author details

[1]Rock Mechanics Laboratory, 101 Terry Fuller Petroleum Engineering Research Building, Texas Tech University, Lubbock, TX, USA. [2]Bob L. Herd Department of Petroleum

Engineering, Texas Tech University, Lubbock, TX, USA. [3]School of Geosciences, University of Oklahoma, Norman, OK, USA. [4]BP America Inc., Houston, TX, USA. [5]EPSLOG S.A., Liege, Belgium. [6]Department of Chemical Engineering, University of Utah, Salt Lake City, UT, USA.

References

Akono AT, Kabir P. Microscopic fracture characterization of gas shale via scratch testing. Mechanics Research Communications. 2016;78:86-92.

Akono AT. Assessment of fracture properties and rate effects on fracture of materials by micro scratching: application to gas shale. Massachusetts Institute of Technology. 2013;69-76.

Al-Shayea NA, Khan K, Abduljauwad SN. Effects of confining pressure and temperature on mixed-mode (I–II) fracture toughness of a limestone rock. International Journal of Rock Mechanics and Mining Sciences. 2000:37(4):629-643. https://doi.org/10.1016/S1365-1609(00)00003-4.

Al-Shayea NA. Effect of testing methods and conditions on the elastic properties of limestone rock. Eng Geol. 2004;74:139-156. https://doi.org/10.1016/j.enggeo.2004.03.007.

Balme MR, Rocchi V, Jones C, Sammonds PR, Meredith PG, Boon S. Fracture toughness measurements on igneous rocks using a high-pressure, high-temperature rock fracture mechanics cell. Journal of Volcanology and Geothermal Research. 2004;132:159-172. https://doi.org/10.1016/S0377-0273(03)00343-3.

Belyadi H, Fathi E, Belyadi F. Chapter Thirteen - Rock mechanical properties and in situ stresses. In: Belyadi H, Fathi E, Belyadi F, editors. Hydraulic Fracturing in Unconventional Reservoirs (Second Edition). Gulf Professional Publishing; 2019. p. 215-231. https://doi.org/10.1016/B978-0-12-817665-8.00013-8.

Bhagat RB. Mode I fracture toughness of coal. International Journal of Mining Engineering. 1985;3:229–236. https://doi.org/10.1007/BF00880769.

Brindley, GW. Phyllosilicates. In: Mineralogy. Encyclopedia of Earth Science. Springer, Boston, MA; 1981. https://doi.org/10.1007/0-387-30720-6_100.

Callahan OA, Eichhubl P, Davatzes NC. Mineral precipitation as a mechanism of fault core growth. Journal of Structural Geology. 2020;140. https://doi.org/10.1016/j.jsg.2020.104156

Callahan OA, Eichhubl P, Olson JE, Davatzes NC. Experimental Investigation of Chemically Aided Fracture Growth in Silicified Fault Rocks. Geothermics. 2019a;83. https://doi.org/10.1016/j.geothermics.2019.101724

Callahan OA, Eichhubl P, Olson JE, Davatzes NC. Fracture Mechanical Properties of Damaged and Hydrothermally Altered Rocks, Dixie Valley-Stillwater Fault Zone, Nevada, USA. J

462 Geophys Res Solid Earth. 2019b;124(4):4069-4090.
463 https://doi.org/10.1029/2018JB016708

464 Campbell DA, Morris CW, Verity RV. Geothermal Well Stimulation Experiments and
465 Evaluation. Society of Petroleum Engineers. 1981. https://doi.org/10.2118/10316-MS

466 Carpenter BM, Scuderi MM, Collettini C, Marone C. Frictional heterogeneities on carbonate-
467 bearing normal faults: Insights from the Monte Maggio Fault, Italy. J Geophys Res Solid Earth.
468 2014;119(12):9062-9076. https://doi.org/10.1002/2014JB011337

469 Chen S, Yue ZQ, Tham LG. Digital image-based numerical modeling method for prediction of
470 inhomogeneous rock failure. Int J Rock Mech Min Sci. 2004;41:939-957.
471 https://doi.org/10.1016/j.ijrmms.2004.03.002.

472 Cheng Y, Chen X. Characteristics of Seismicity inside and outside the Salton Sea Geothermal
473 Field. Bulletin of the Seismological Society of America. 2018;108(4):1877-1888.
474 https://doi.org/10.1785/0120170311

475 Coudyzer C, Poyol E, Bette P, Dagrain F. Measure of rock mechanical properties from
476 scratching test. In: AAPG International Conferences and Exhibition. 2005

477 Crandall D, Gill M, Moore J, Brown S, Mackey P. The Influence of Micro-Fabric Heterogeneity
478 on Sheared Rock Properties. Unconventional Resources Technology Conference. 2019.
479 https://doi.org/10.15530/urtec-2019-926

480 Dagrain F, Germay C. Fields applications for the scratching tests. In: The Eurock 2006:
481 Multiphysics Coupling and Long Term Behaviour in Rock Mechanics. 2006;571-576.

482 Dagrain F, Richard T, Germay C. The Rock Strength Device: A scratching apparatus to
483 determine rock properties. In: The 7th National Congress on theoretical and applied
484 Mechanics, NCTAM. 2006.

485 Dalamarinis P, Kelessidis VC, Chatzistamou V, Karydakis G, Chlaboutakis M. Analysis of water
486 and geothermal-well shallow drilling data via drilling software allows for rock drillability
487 assessment and drill bit performance. In: 3rd AMIREG International Conference: Assessing
488 the Footprint of Resource Utilization and Hazardous Waste Management, Athens, Greece.
489 2009.

490 Deere DU. Geological considerations. In: Stagg KG, Zienkiewicz OC, editors. Rock mechanics
491 in engineering practice. London: Wiley; 1968. p. 1-20.

492 Detournay E, Defourny P. A phenomenological model for the drilling action of drag bits.
493 International Journal of Rock Mechanics and Mining Sciences and Geomechanics Abstracts.
494 1992;29:13-23. https://doi.org/10.1016/0148-9062(92)91041-3

495 Diehl T, Kraft T, Kissling E, Wiemer S. The induced earthquake sequence related to the st.
496 gallen deep geothermal project (Switzerland): fault reactivation and fluid interactions
497 imaged by microseismicity. J Geophys Res Solid Earth. 2017;122(9).
498 https://doi.org/10.1002/2017jb014473

499 Dotsey P, Deighton I. New approach to basin formation temperature modelling. First break.
500 2012;30.

501 Eddine MJ. Measurement of fracture toughness, mechanical and electrical loss tangents of
502 calcium carbonate reinforced vinyl ester composites. USQ Project.
503 https://eprints.usq.edu.au/8397 (2009) Accessed 17 June 2020.

504 Erdlac Jr RJ, Swift DB. Deep Permeable Strata Geothermal Energy (DPSGE): Tapping Giant
505 Heat Reservoirs within Deep Sedimentary Basins-An Example From Permian Basin
506 Carbonate Strata. GRC Transactions. 2004;28.

507 Erdlac Jr RJ. A Resource Assessment of Geothermal Energy Resources for Converting Deep
508 Gas Wells in Carbonate Strata into Geothermal Extraction Wells: A Permian Basin Evaluation.
509 U.S. Department of Energy Office of Energy Efficiency and Renewable Energy, EERE.
510 https://doi.org/10.2172/893183 (2006) Accessed 17 June 2020.

511 Finnila A, Dershowitz W, Doe T, McLaren, R. Hydro-Shearing and Hydraulic Fracturing for
512 Enhanced Geothermal Systems in Archetypical Normal, Strike-Slip and Thrust Faulting
513 Terrains. GRC Transactions. 2015;39:1-19.

514 Frash, LP, Gutierrez MS, Hampton JC. Experimentation with Hydraulic Impulse Stimulation
515 in a Scaled Enhanced Geothermal Systems Reservoir. American Rock Mechanics Association,
516 ARMA-2013-166. 2013.

517 Funatsu T, Seto M, Shimada H, Matsui K, Kuruppu M. Combined effects of increasing
518 temperature and confining pressure on the fracture toughness of clay bearing rocks.
519 International Journal of Rock Mechanics and Mining Sciences. 2004;41(6):927-938.
520 https://doi.org/10.1016/j.ijrmms.2004.02.008.

521 Germay C, Lhomme T, McPhee C, Daniels G. An Objective Review of Non-Destructive Methods
522 for the Direct Testing of Strength on Rock Cores. American Rock Mechanics Association.
523 2018.

524 Germay C, Richard T, Mappanyompa E, Lindsay C, Kitching D, Khaksar A. The Continuous-
525 Scratch Profile: A High-Resolution Strength Log for Geomechanical and Petrophysical
526 Characterization of Rocks. Society of Petroleum Engineers. 2015.

527 Gholizadeh Doonechaly N, Rahman SS, Kotousov A. A New Approach to Hydraulic
528 Stimulation of Geothermal Reservoirs by Roughness Induced Fracture Opening. In: Bunger
529 AP, McLennan J, Jeffrey R, editors. Effective and Sustainable Hydraulic Fracturing. London:
530 IntechOpen; 2013. p. 573-590. http://doi.org/10.5772/56447

531 Gokceoglu C, Zorlu K. A fuzzy model to predict the uniaxial compressive strength and
532 modulus of elasticity of problematic rocks. Eng Appl Artif Intell. 2004;17(1):61–72.
533 https://doi.org/10.1016/j.engappai.2003.11.006.

534 Gunsallus KL, Kulhawy FH. A comparative evaluation of rock strength measures.
535 International Journal of Rock Mechanics and Mining Sciences & Geomechanics Abstracts.
536 1984;21(5):233-248. https://doi.org/10.1016/0148-9062(84)92680-9.

Han S, Cheng Y, Gao Q, Yan C, Wei J, Zhang J. Simulation Study on Heat Extraction in Enhanced Geothermal Reservoirs with Random Fracture Distribution. American Rock Mechanics Association, ARMA-2019-1857. 2019.

Handin J, Carter N. Rheology of rocks. In: Structural Geology and Tectonics. Encyclopedia of Earth Science. Springer: Berlin; 1987. https://doi.org/10.1007/3-540-31080-0_87.

Hantler A. Crushing index – Aitik. Technical Report, no. 8HX286586.10, Pöyry Sweden AB. 2015.

Hoek E, Martin CD. Fracture initiation and propagation in intact rock-a review. J Rock Mech Geotech Eng. 2014;6(4):287-300. https://doi.org/10.1016/j.jrmge.2014.06.001

Ishibashi T, Watanabe N, Asanuma H, Watanabe K. Preliminary Investigation of the Hydraulic Stimulation for a Field-Scale Forge Candidate Geothermal Reservoir. Society of Petrophysicists and Well-Log Analysts, SPWLA-JFES-2019-D. 2019.

Kaplan U. Organic Rankine Cycle Configurations. In: European Geothermal Congress, Unterhaching, Germany. 2007.

Kerr Jr SD, Thomson A. Origin of Nodular and Bedded Anhydrite in Permian Shelf Ssdiments, Texas and New Mexico. AAPG Bulletin. 1963;47. https://doi.org/10.1306/BC743B0B-16BE-11D7-8645000102C1865D

Kolawole F, Johnston CS, Morgan CB, Chang JC, Marfurt KJ, Lockner DA, Reches Z, Carpenter BM. The susceptibility of Oklahoma's basement to seismic reactivation. Nature Geoscience. 2019;12:839-844. https://doi.org/10.1038/s41561-019-0440-5

Kolawole O, Ispas I. Evaluation of Geomechanical Properties Via Scratch Tests: Where Are We and Where Do We Go from Here?. SN Applied Sciences. 2020b;2(10). http://doi.org/10.1007/s42452-020-03469-5

Kolawole O, Ispas I. Interaction between hydraulic fractures and natural fractures: current status and prospective directions. Journal of Petroleum Exploration and Production Technology. 2020a;10:1613-1634. https://doi.org/10.1007/s13202-019-00778-3

Kolawole O. Scratch Test Characterization of Heterogeneous Rock Mechanical Properties with Applications to Enhanced Geothermal Systems. Mendeley Data. 2020;v2. https://doi.org/10.17632/xwhnkzzdmm.2

Majdi A, Rezaei M. Prediction of unconfined compressive strength of rock surrounding a roadway using artificial neural network. Neural Comput & Applic. 2013;23:381-389. https://doi.org/10.1007/s00521-012-0925-2.

McClure MW, Horne RN. An Investigation of Stimulation Mechanisms in Enhanced Geothermal Systems. International Journal of Rock Mechanics & Mining Sciences. 2014;72:242-60. https://doi.org/10.1016/j.ijrmms.2014.07.011

McClure MW, Horne, RN. Is Pure Shear Stimulation Always the Mechanism of Stimulation in EGS?. In: Thirty-Eighth Workshop on Geothermal Reservoir Engineering, Stanford University, California. 2013.

575 Meller C, Kohl T. The significance of hydrothermal alteration zones for the mechanical
576 behavior of a geothermal reservoir. Geothermal Energy. 2014;2:12.
577 https://doi.org/10.1186/s40517-014-0012-2

578 Mitaim S, Dagrain F, Richard T, Detournay E, Drescher A. A novel apparatus to determine the
579 rock strength parameters. In: The 9th National Convention on Civil Engineering, Thailand.
580 2004.

581 Murphy HD, Lawton RG, Tester JW, Potter RM, Brown DW, Aamodt RL. Preliminary
582 Assessment of a Geothermal Energy Reservoir Formed by Hydraulic Fracturing. Society of
583 Petroleum Engineers. 1977.

584 Nadimi S, Forbes B, Moore J, Podgorney R, McLennan JD. Utah FORGE: Hydrogeothermal
585 modeling of a granitic based discrete fracture network. Geothermics. 2020;87.
586 https://doi.org/10.1016/j.geothermics.2020.101853

587 Nataraj MS. Preliminary Geotechnical Evaluation of Deep Borehole Facilities for Nuclear
588 Waste Disposal in Shales. In: Bennett RH, et al. editors. Microstructure of Fine-Grained
589 Sediments. Frontiers in Sedimentary Geology. New York, NY: Springer; 1991.
590 https://doi.org/10.1007/978-1-4612-4428-8_57.

591 Palchik V. Influence of porosity and elastic modulus on uniaxial compressive strength in soft
592 brittle porous sandstones. Rock Mech Rock Eng. 1999;32(4):303–309.
593 https://doi.org/10.1007/s006030050050.

594 Palchik, V. On the Ratios between Elastic Modulus and Uniaxial Compressive Strength of
595 Heterogeneous Carbonate Rocks. Rock Mech Rock Eng. 2011;44:121-128.
596 https://doi.org/10.1007/s00603-010-0112-7.

597 Pine RJ, Batchelor AS. Downward Migration of Shearing in Jointed Rock During Hydraulic
598 Injections. International Journal of Rock Mechanics & Mining Sciences & Geomechanics
599 Abstracts. 1984;21:249-63. https://doi.org/10.1016/0148-9062(84)92681-0

600 Quoilin S, Van Den Broek M, Declaye S, Dewallef P, Lemort V. Techno-economic survey of
601 Organic Rankine Cycle (ORC) systems. Renew Sust Energ Rev. 2013;22:168-186.
602 https://doi.org/10.1016/j.rser.2013.01.028

603 Riahi A, Radakovic-Guzina Z, Damjanac B, Katsaga T. Three-dimensional Numerical
604 Investigation of the Effect of Injection Method on Shear Stimulation of Enhanced Geothermal
605 Reservoirs. American Rock Mechanics Association, ARMA-2015-869. 2015.

606 Richard T, Dagrain F, Poyol E, Detournay E. Rock strength determination from scratch tests.
607 Engineering Geology. 2012;147-148:91-100.

608 Ruppel SC, Jones RH, Breton CL, Kane JA. Preparation of maps depicting geothermal gradient
609 and Precambrian structure in the Permian basin. In: USGS Order no. 04CRSA0834 and
610 Requisition no. 04CRPR01474. 2005.

611 Saller A, Bierly L, Shafer D, Owens L. Contrasting Styles of San Andres Reservoirs: Vacuum
612 Versus Slaughter Fields, Middle Permian, West Texas and Southeast New Mexico. In: AAPG
613 Annual Convention and Exhibition. 2012.

614 Schei G, Fjær E, Detournay E, Kenter CJ, Fuh GF, Zausa F. The Scratch Test: An Attractive
615 Technique for Determining Strength and Elastic Properties of Sedimentary Rocks. Society of
616 Petroleum Engineers. 2000.

617 Scholz CH. Experimental study of the fracturing process in brittle rock. Journal of
618 Geophysical Research. 1968a;73(4). https://doi.org/10.1029/JB073i004p01447.

619 Scholz CH. Microfracturing and the inelastic deformation of rock in compression. Journal of
620 Geophysical Research. 1968b;73(4). https://doi.org/10.1029/JB073i004p01417.

621 Shao H, Hein P, Sachse A, Kolditz O 2016. Geoenergy Modeling II: Shallow Geothermal
622 Systems. Springer Briefs in Energy: Computational Modeling of Energy Systems;2016.
623 https://doi.org/10.1007/978-3-319-45057-5.

624 Sheng M, Xu Z, Wang X, Li P. Experimental Study on Hydro-shearing Propagation of an
625 Embedded Fracture in Hot Dry Granite Rock. GRC Transactions. 2018;42.

626 Sleep NH. Hydrothermal circulation, anhydrite precipitation, and thermal structure at ridge
627 axes. J Geophys Res Solid Earth. 1991;96:2375-2387. https://doi.org/10.1029/90JB02335

628 Sonmez H, Tuncay E, Gokceoglu C. Models to predict the uniaxial compressive strength and
629 the modulus of elasticity for Ankara agglomerate. Int J Rock Mech Min Sci. 2004;41(5):717-
630 729. https://doi.org/10.1016/j.ijrmms.2004.01.011

631 Stober I, Bucher K. Enhanced-Geothermal-Systems, Hot-Dry-Rock Systems, Deep-Heat-
632 Mining. In: Geothermal Energy. Berlin: Springer;2013. https://doi.org/10.1007/978-3-642-
633 13352-7_9

634 Suarez-Rivera R, Stenebråten J, Dagrain F. Continuous Scratch Testing on Core Allows
635 Effective Calibration of Log-Derived Mechanical Properties for Use in Sanding Prediction
636 Evaluation. Society of Petroleum Engineers. 2002. https://doi.org/10.2118/78157-MS

637 Tang CM. Permian Basin. Encyclopædia Britannica. 2015.
638 https://www.britannica.com/place/Permian-Basin

639 Teagle DAH, Alt JC, Halliday AN. Tracing the chemical evolution of fluids during
640 hydrothermal recharge: Constraints from anhydrite recovered in ODP Hole 504B. Earth and
641 Planetary Science Letters. 1998;155:167-182. https://doi.org/10.1016/S0012-
642 821X(97)00209-4.

643 Tesei T, Collettini C, Carpenter BM, Viti C, Marone C. Frictional strength and healing behavior
644 of phyllosilicate-rich faults. Journal of Geophysical Research. 2012;117:B09402.
645 https://doi.org/10.1029/2012JB009204.

646 Tham LG, Cheung YK, Tang CA. Numerical Simulation of the Failure Process of Rocks.
647 Tamkang Journal of Science and Engineering. 2001;4:239-252.

Toth AN. Country Update for Hungary. In: World Geothermal Congress, Reykjavik, Iceland. 2020.

Wang F, Konietzky H, Herbst M. Influence of heterogeneity on thermo-mechanical behaviour of rocks. Comput Geotech. 2019;116. https://doi.org/10.1016/j.compgeo.2019.103184.

Wang H. Numerical investigation of fracture spacing and sequencing effects on multiple hydraulic fracture interference and coalescence in brittle and ductile reservoir rocks. Engineering Fracture Mechanics. 2016;157:107-124. https://doi.org/10.1016/j.engfracmech.2016.02.025.

Wang H. Numerical modeling of non-planar hydraulic fracture propagation in brittle and ductile rocks using XFEM with cohesive zone method. Journal of Petroleum Science and Engineering. 2015;135:127-140. https://doi.org/10.1016/j.petrol.2015.08.010.

Wang X, Ghassemi A. A 3D Thermal-Poroelastic Model for Naturally Fractured Geothermal Reservoir Stimulation. American Rock Mechanics Association. 2012.

Wiemer S, Kraft T, Trutnevyte E, Roth P. "Good Practice" Guide for Managing Induced Seismicity in Deep Geothermal Energy Projects in Switzerland. SED, Swiss Seismological Service at ETH Zürich. 2017. https://doi.org/10.3929/ethz-b-000254161

Yao W, Xu Y, Xia K., et al. Dynamic Mode II Fracture Toughness of Rocks Subjected to Confining Pressure. Rock Mech Rock Eng. 2020;53:569-586. https://doi.org/10.1007/s00603-019-01929-y

Yao Y. Linear Elastic and Cohesive Fracture Analysis to Model Hydraulic Fracture in Brittle and Ductile Rocks. Rock Mech Rock Eng. 2012;45:375-387. https://doi.org/10.1007/s00603-011-0211-0.

Yılmaz I, Sendır H. Correlation of Schmidt hardness with unconfined compressive strength and Young's modulus in gypsum from Sivas (Turkey). Engineering Geology. 2002;66,:211-219. https://doi.org/10.1016/S0013-7952(02)00041-8.

Zbinden D, Rinaldi AP, Diehl T, Wiemer S. Hydromechanical Modeling of Fault Reactivation in the St. Gallen Deep Geothermal Project (Switzerland): Poroelasticity or Hydraulic Connection?. Geophysical Research Letters. 2020;47. https://doi.org/10.1029/2019GL085201

Zhang H, Huang Z, Zhang S, Yang Z, Mclennan JD. Improving heat extraction performance of an enhanced geothermal system utilizing cryogenic fracturing. Geothermics. 2020;85. https://doi.org/10.1016/j.geothermics.2020.101816

Zhang JJ. Chapter 4 - Basic rock fracture mechanics. In: Zhang JJ, editors. Applied Petroleum Geomechanics. Gulf Professional Publishing; 2019. p.33-161. https://doi.org/10.1016/B978-0-12-814814-3.00004-6.

Zhang ZX, Yu J, Kou SQ, Lindqvist P-A. Effects of high temperatures on dynamic rock fracture. International Journal of Rock Mechanics and Mining Sciences. 2001;38:211-225. https://doi.org/10.1016/S1365-1609(00)00071-X.

686 Zhang Z-X. Chapter 5 - Effect of Temperature on Rock Fracture. In: Zhang Z-X, editors. Rock
687 Fracture and Blasting: Theory and Applications. Elsevier Inc; 2016. p. 111-133.
688 https://doi.org/10.1016/B978-0-12-802688-5.00005-1.

689 Zhou Z, Jin Y, Zeng Y, Youn D. Experimental Study of Hydraulic Fracturing in Enhanced
690 Geothermal System. American Rock Mechanics Association. 2018.

691 Ziegler MO, Heidbach O. The 3D stress state from geomechanical–numerical modelling and
692 its uncertainties: a case study in the Bavarian Molasse Basin. Geothermal Energy. 2020;8:11.
693 https://doi.org/10.1186/s40517-020-00162-z

694 Zoback MD. (2010) Reservoir Geomechanics. Cambridge University Press. New York:
695 Cambridge University Press; 2010.

696

697

698

699

700

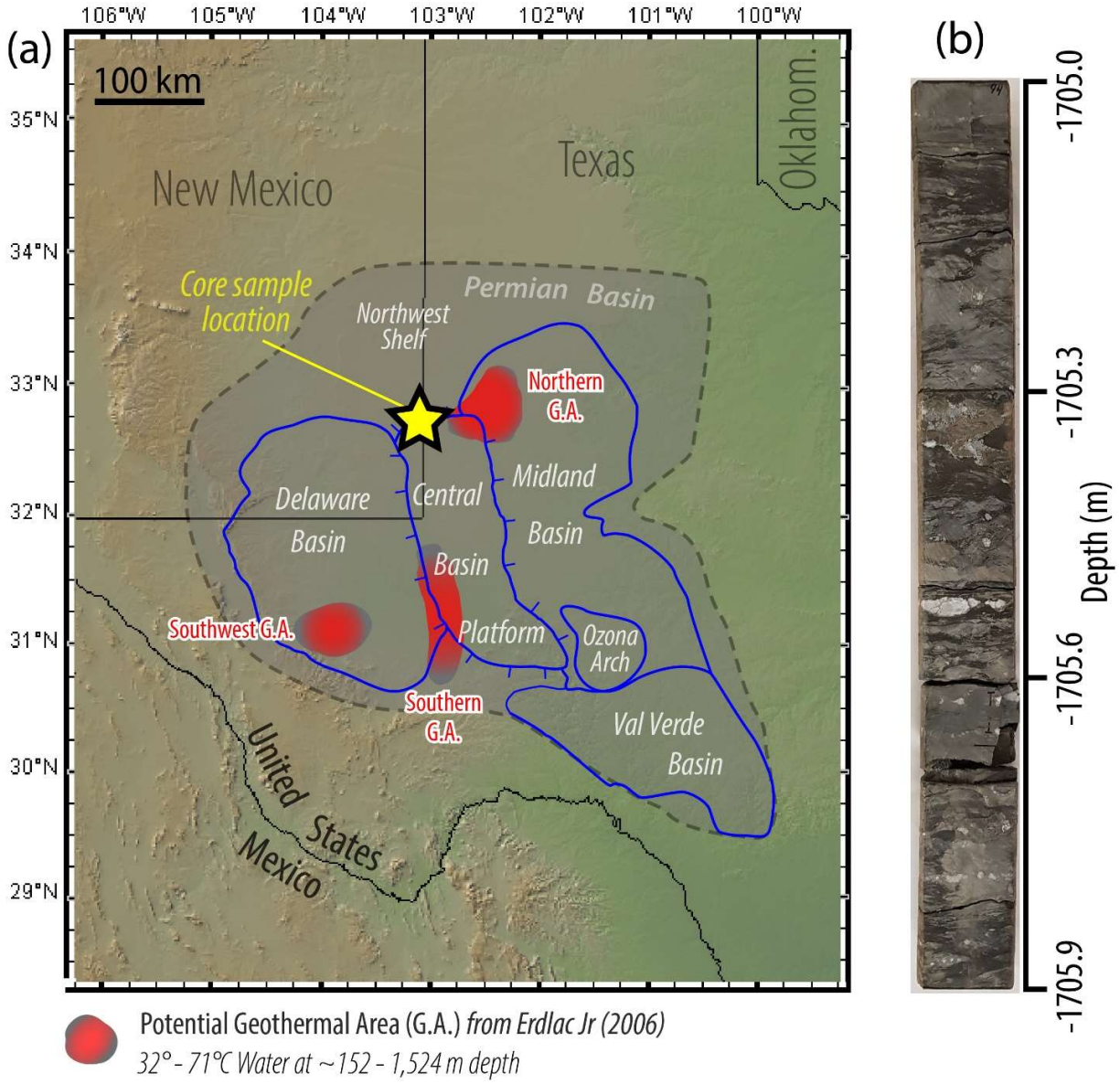

701

702 **Fig. 1.** (a) Map of Permian Basin, U.S., showing the locations of potential geothermal areas
703 and location of (b) the core sample analyzed in this study.

704

705

706

707

708

709

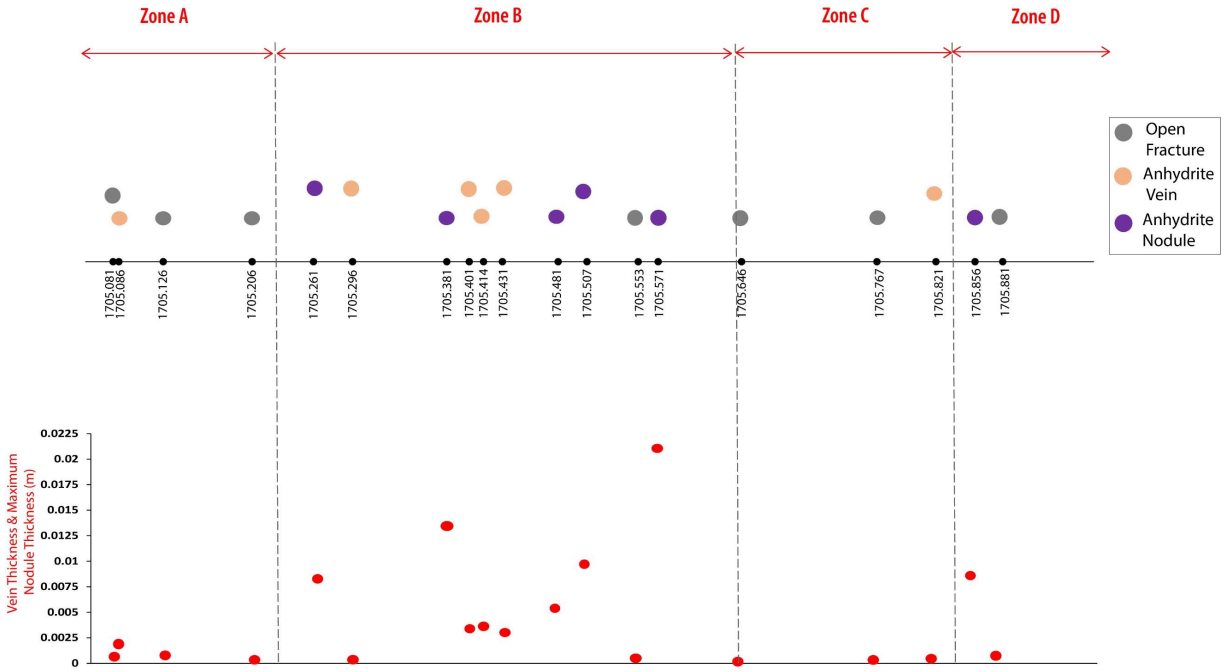

Fig. 2. Result of core-scale characterization of the post-diagenetic alterations in the rock.

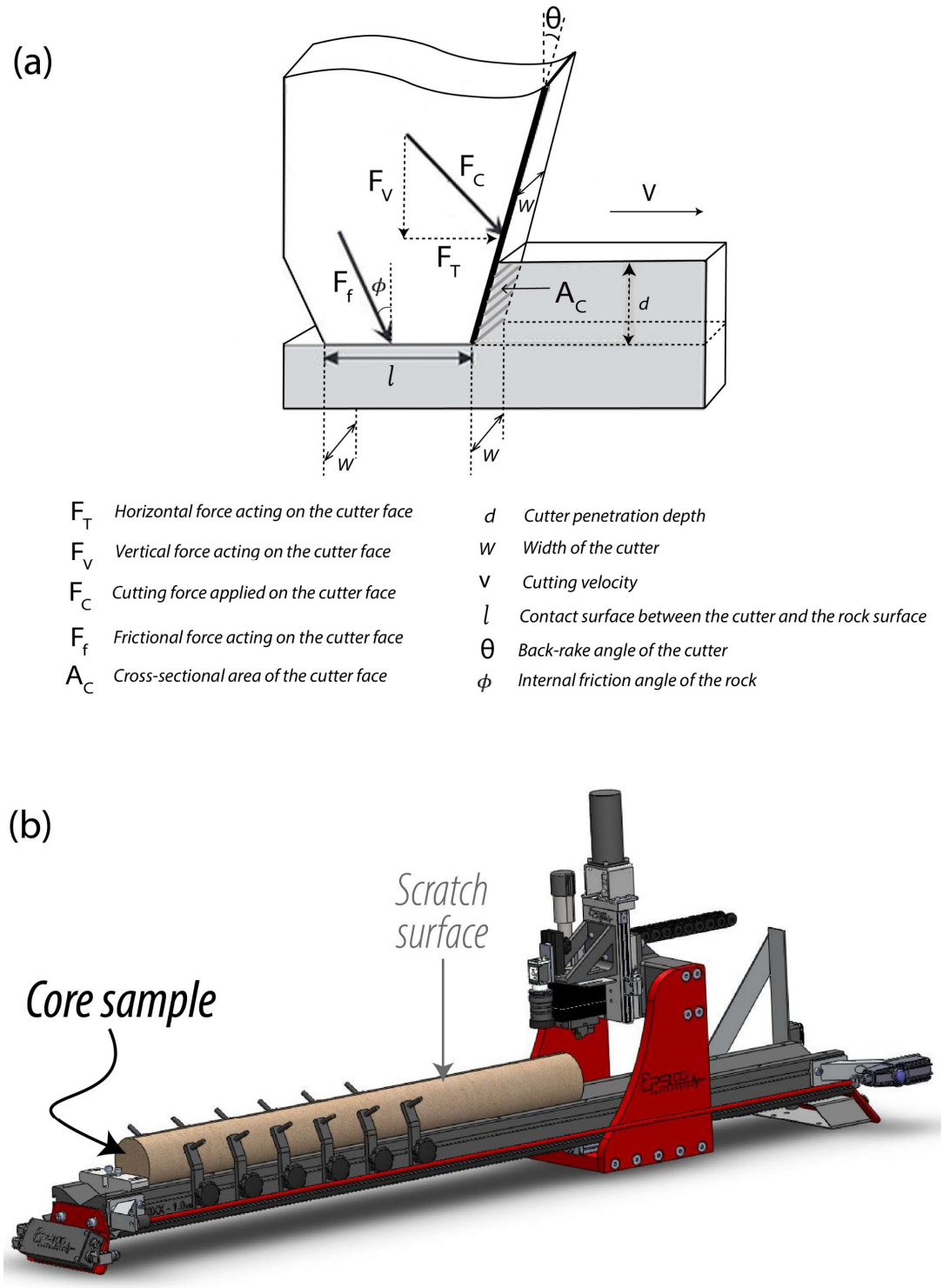

Fig. 3. The Scratch Test Schematic. (a) Rock scratching configuration for a sharp cutter. (b) Epslog Wombat machine (Pre-modified image courtesy of Epslog S.A.).

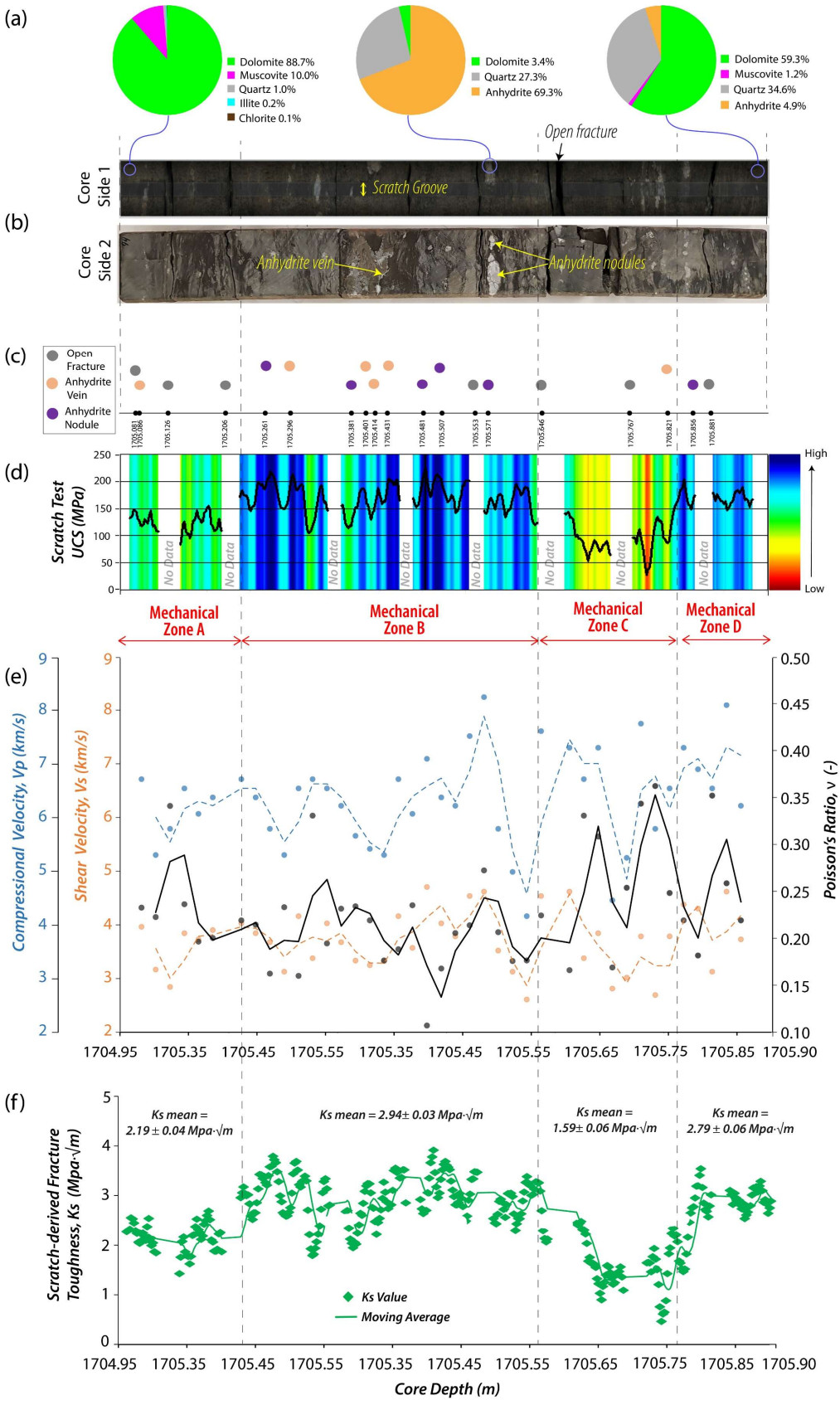
(a)
Dolomite 88.7%
Muscovite 10.0%
Quartz 1.0%
Illite 0.2%
Chlorite 0.1%
Dolomite 3.4%
Quartz 27.3%
Anhydrite 69.3%
Dolomite 59.3%
Muscovite 1.2%
Quartz 34.6%
Anhydrite 4.9%
Open fracture
Core Side 1
Scratch Groove
(b)
Core Side 2
Anhydrite vein
Anhydrite nodules
(c)
Open Fracture
Anhydrite Vein
Anhydrite Nodule
(d)
Scratch Test UCS (MPa)
No Data
High
Low
Mechanical Zone A
Mechanical Zone B
Mechanical Zone C
Mechanical Zone D
(e)
Compressional Velocity, Vp (km/s)
Shear Velocity, Vs (km/s)
Poisson's Ratio, ν (-)
(f)
Scratch-derived Fracture Toughness, Ks (Mpa·√m)
Ks mean = 2.19 ± 0.04 Mpa·√m
Ks mean = 2.94± 0.03 Mpa·√m
Ks mean = 1.59± 0.06 Mpa·√m
Ks mean = 2.79 ± 0.06 Mpa·√m
Ks Value
Moving Average
Core Depth (m)

Fig. 4. (a) X-ray Diffraction (XRD) analysis of the core sample; (b) Digital photography of core sample; (c) Core-scale characterization; (d) Scratch test unconfined compressive strength (UCS); (e) Ultrasonic shear and compressional velocities, and dynamic Poisson's ratio; (f) Scratch-derived fracture toughness.

Figures

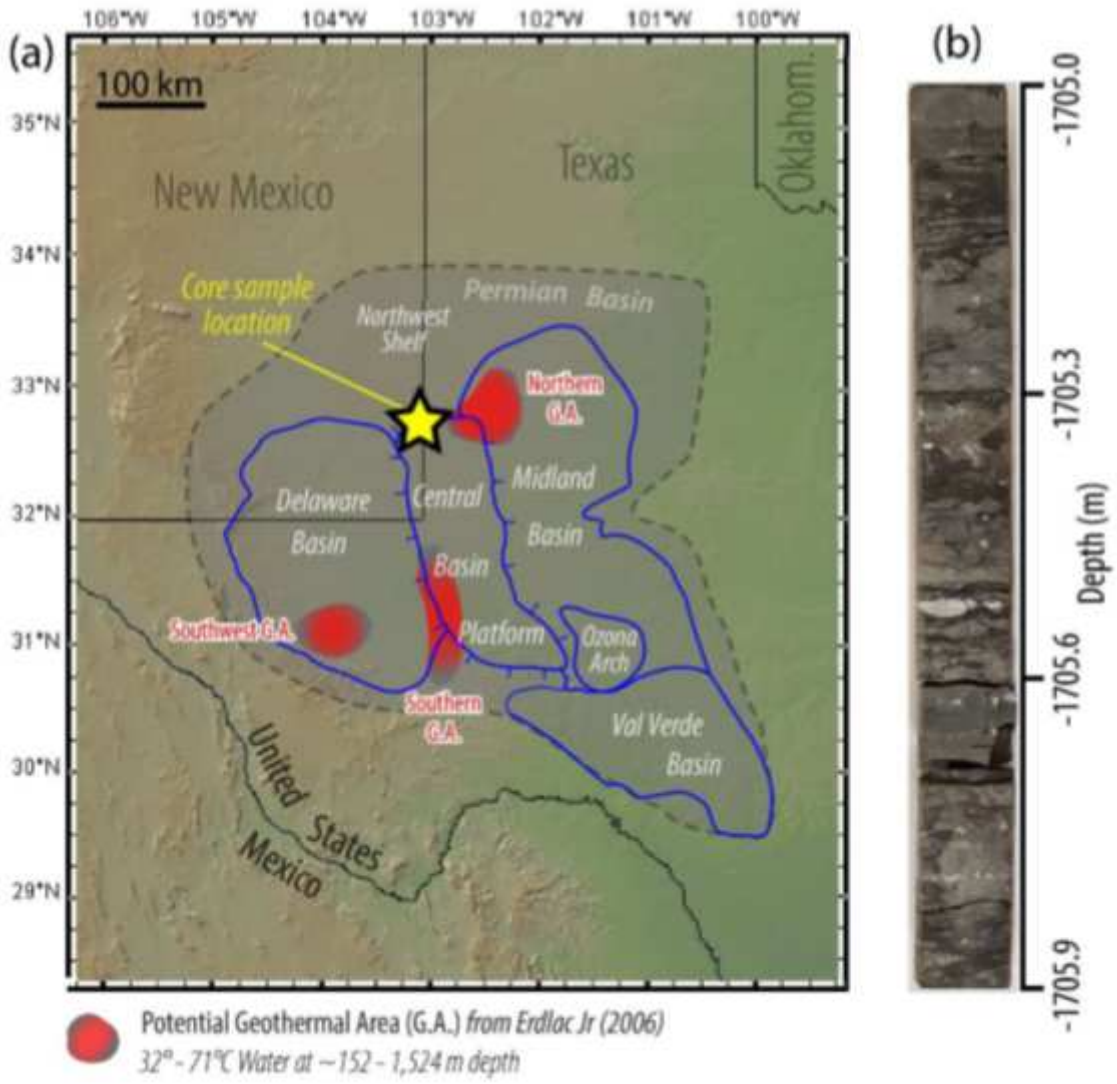

Figure 1

(a) Map of Permian Basin, U.S., showing the locations of potential geothermal areas and location of (b) the core sample analyzed in this study.

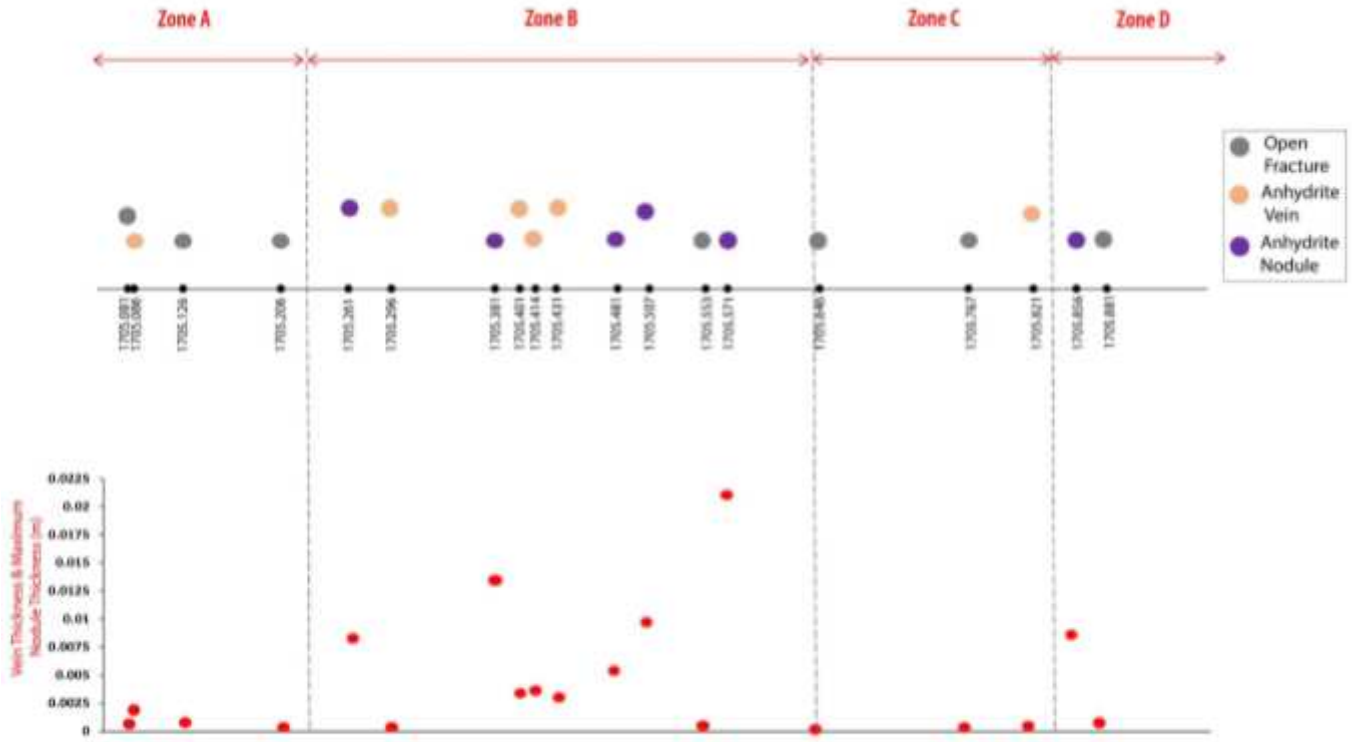

Figure 2

Result of core-scale characterization of the post-diagenetic alterations in the rock.

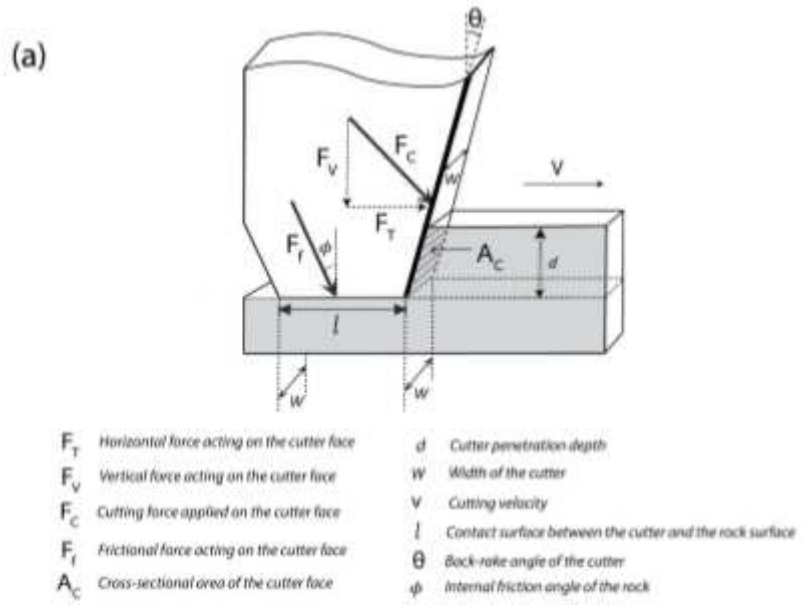

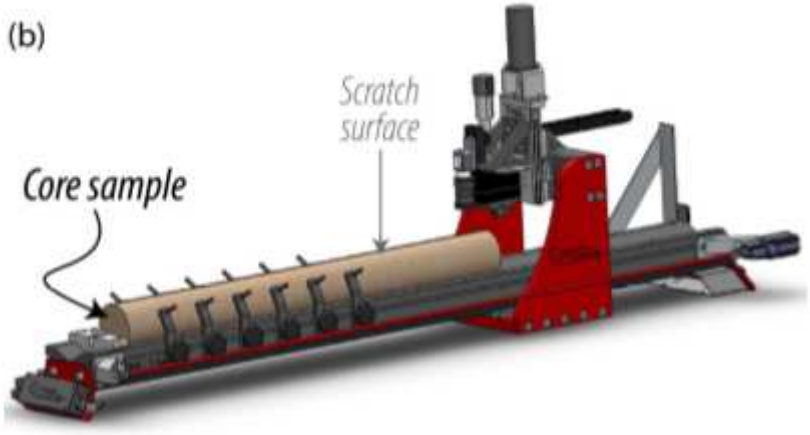

Figure 3

The Scratch Test Schematic. (a) Rock scratching configuration for a sharp cutter. (b) Epslog Wombat machine (Pre-modified image courtesy of Epslog S.A.).

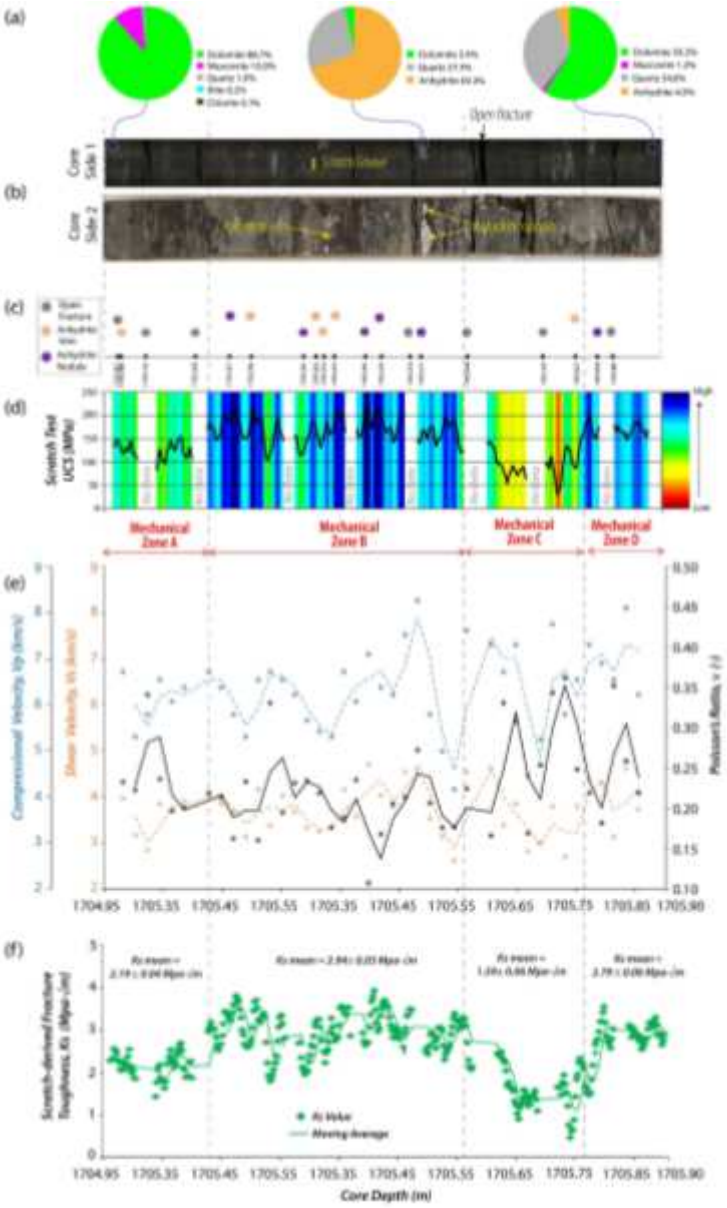

Figure 4

(a) X-ray Diffraction (XRD) analysis of the core sample; (b) Digital photography of core sample; (c) Core-scale characterization; (d) Scratch test unconfined compressive strength (UCS); (e) Ultrasonic shear and compressional velocities, and dynamic Poisson's ratio; (f) Scratch-derived fracture toughness.

Supplementary Files

This is a list of supplementary files associated with this preprint. Click to download.

- SupplementaryInformation.pdf